

Syngas production from glycerol-dry(CO₂) reforming over La-promoted Ni/Al₂O₃ catalyst



Kah Weng Siew^a, Hua Chyn Lee^a, Jolius Gimbut^a, Sim Yee Chin^a, Maksudur R. Khan^a, Yun Hin Taufiq-Yap^b, Chin Kui Cheng^{a,*}

^a Centre of Excellence for Advanced Research in Fluid Flow, Faculty of Chemical & Natural Resources Engineering, Universiti Malaysia Pahang, Lebuhraya Tun Razak, Gambang, Kuantan 26300, Pahang, Malaysia

^b Catalysis Science and Technology Research Centre, Faculty of Science, Universiti Putra Malaysia, UPM Serdang, 43400 Selangor, Malaysia

ARTICLE INFO

Article history:

Received 5 December 2013

Accepted 20 August 2014

Available online

Keywords:

Glycerol

Dry reforming

Lanthanum

Nickel catalyst

Syngas

ABSTRACT

A 3 wt% La-promoted Ni/Al₂O₃ catalyst was prepared via wet co-impregnation technique and physicochemically-characterized. Lanthanum was responsible for better metal dispersion; hence higher BET specific surface area (96.0 m² g⁻¹) as compared to the unpromoted Ni/Al₂O₃ catalyst (85.0 m² g⁻¹). In addition, the La-promoted catalyst possessed finer crystallite size (9.1 nm) whilst the unpromoted catalyst measured 12.8 nm. Subsequently, glycerol dry reforming was performed at atmospheric pressure and temperatures ranging from 923 to 1123 K employing CO₂-to-glycerol ratio from zero to five. Significantly, the reaction results have yielded syngas as main gaseous products with H₂:CO ratios always below than 2.0 with concomitant maximum 96% glycerol conversion obtained at the CO₂-to-glycerol ratio of 1.67. In addition, the glycerol consumption rate can be adequately captured using power law modelling with the order of reactions equal 0.72 and 0.14 with respect to glycerol and CO₂ whilst the activation energy was 35.0 kJ mol⁻¹. A 72 h longevity run moreover revealed that the catalyst gave a stable catalytic performance.

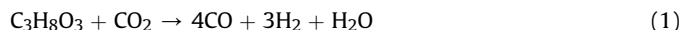
© 2014 Elsevier Ltd. All rights reserved.

1. Introduction

Glycerol steam reforming has been touted as a very promising syngas (mixture of H₂ and CO) production route due to the burgeoning use of biodiesel as a liquid transportation fuel. Nevertheless, the voluminous publications seems to indicate a syngas yield with CO-lean composition [1–6], hence rendering this syngas unsuitable for gasoline production via Fischer-Tropsch synthesis. Most of the earlier studies have ascribed the unsuitable ratio to the water-gas-shift reaction. The use of CO₂, unlike the steam represents a new reforming route with significantly-reduced hydrogen source. Therefore, in theory H₂:CO ratio should be significantly lesser than the steam reforming pathway. Moreover, the kinetics of this reaction is unknown and further research is required.

The alumina supported nickel catalysts have been employed in numerous previous studies for hydrocarbon-based or biomass-based reformation into syngas [7–10]. However, Ni-based

catalysts are prone to the carbon deposition. To mitigate carbon laydown, the promoters such as La-metal has been employed [11–15]. In particular, it has been reported before that the La promoted catalysts possessed higher catalytic reactivity and successfully reduced the carbon deposition [16,17]. Significantly, the increase of anti-coking property has been attributed to the factors such as the size of particle as well as the redox properties of La [18]. Therefore, in the current work, an alumina supported nickel catalyst promoted with 3.0 wt% La was synthesized and employed in glycerol dry reforming as in Eq. (1).



2. Experimental

2.1. Catalyst preparation

The alumina support was purchased from Sigma Aldrich and air-calcined at 1073 K for 6 h. Subsequently, it was sieved to the particle size of 140–425 μm. For the catalyst preparation, an accurately weighed calcined alumina was mixed with Ni(NO₃)₂·6H₂O and

* Corresponding author. Tel.: +60 9 549 2896; fax: +60 9 549 2889.

E-mail addresses: chinkui@ump.edu.my, cheng.chinkui@gmail.com (C.K. Cheng).

La(NO₃)₃·6H₂O aqueous solutions and then magnetically-stirred for 3 h. It was later dried at 373 K for 12 h to obtain 3 wt% La–20 wt%Ni/77 wt% Al₂O₃ catalyst. The dried catalyst was then air-calcined at 1073 K for 5 h. Finally, it was ground and sieved to particle range of 140–250 μm for physicochemical characterization and reaction studies. For physicochemical property comparisons, 20 wt%Ni/80 wt% Al₂O₃ was also prepared employing the aforementioned procedures.

2.2. Catalyst characterization

Liquid N₂ with a cross-sectional area of 0.162 nm² was used as an adsorbate for adsorption/desorption cycles performed at 77 K for the determination of surface area and pore volume of solid catalysts. The crystalline structure was obtained via XRD diffraction analysis. The samples were irradiated by Ni-filtered CuK_α with a wavelength (λ) of 1.542 Å at 40 mA and 45 kV, and scanning from 10° to 80° at 4° min^{−1} employing Rigaku Miniflex II XRD instrument. The temperature-programmed reduction (TPR) profiles of freshly-calcined catalysts under H₂-blanket were carried out using IP Thermo Electron TPDRO series 1100. Furthermore, TGA unit (Q500-series model) was utilized to determine the non-isothermal oxide-metal formation from the decomposition of metal nitrate precursor of the uncalcined solid catalyst samples. For each analysis, the catalysts were ramped at 10, 15 and 20 K min^{−1} respectively to 1173 K and held for 1 h under the 50 ml min^{−1} of high purity air. For the used catalysts (collected post-reaction), the temperature-programmed-oxidation (TPO) profiles under O₂ blanket were obtained. TPO analyses were performed with ramping rate fixed at 10 K min^{−1} to reach 1173 K followed by an hour holding period. In addition, the morphology and bulk composition were examined with JEOL/JSM-7800F Thermal FESEM instrument. The accelerating voltage employed for the experiment was in the range of 5–15 kV.

2.3. Catalyst evaluation

All the glycerol dry reforming experiments were conducted in a stainless-steel fixed bed reactor (ID = 0.9525 cm; length = 40 cm) positioned inside a tubular furnace (cf. Fig. 1). Catalyst bed was supported by quartz wool on a stainless steel support welded to the internal wall of reactor tubing. The performance of each catalyst was evaluated from 923 to 1123 K and at 1 atm pressure. Liquid glycerol at a pre-determined flowrate was injected into the vaporizer upstream of the reactor with a HPLC pump (Lab Alliance Series 1). Prior to the testing, catalyst was reduced by H₂ (50 ml min^{−1} STP) for 2 h with heating ramp at 10 K min^{−1}. All the inlet gas flow rates were regulated by the electronic mass flow controller (Alicat Series). The total inlet flow was fixed at a weight-hourly-space-velocity (WHSV) of 3.6 × 10⁴ ml g^{−1} h^{−1} STP. Reactor outlet gases were passed through a cold trap for liquid products capture and then over a drierite (CaSO₄) bed (8 mesh). The exit gas was collected into a 1-L Tedlar gas sampling bag. The composition of syngas produced was determined using Agilent gas chromatography (GC) with TCD capillary columns, HP-MOLSIV (Model No. Agilent 19095P; 30.0 m × 530 μm × 50.0 μm) and HP-Plot/Q column (Model No. Agilent 19095-Q04; 30.0 m × 530 μm × 40.0 μm). He was used as the carrier gas. Product stream flow rate was measured using a bubble meter. Glycerol consumption was calculated based on the atomic H balance for the formation of atom H-containing gaseous species, viz. H₂ and CH₄. In order to approximate the plug flow conditions and minimize the back-mixing or channelling, the ratio of catalyst bed length to catalyst particle diameter (L/d_p) was 80 and the ratio of inner diameter of reactor to particle diameter (d_t/d_p) was 71.5. The catalytic performance was

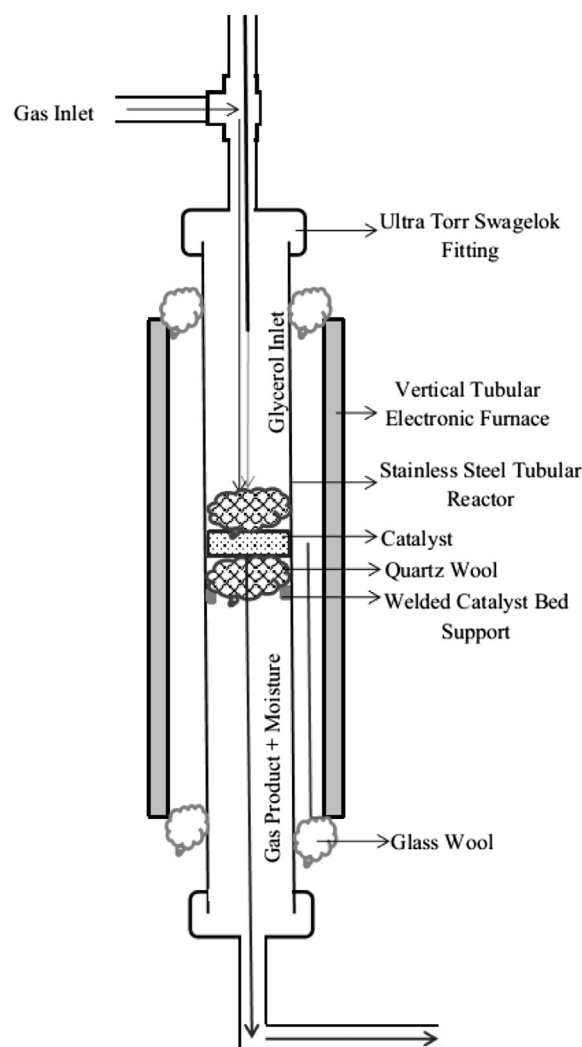


Fig. 1. Schematic of the fixed-bed reactor for glycerol dry reforming.

evaluated in terms of gaseous product formations in line with the objective of our current work (cf. Eqs. (2)–(7)). The reaction matrices are:

Product Selectivity.

$$S_{H_2} = \frac{2F_{H_2}}{\frac{8}{3}(F_{CO} + F_{CH_4})} \quad (2)$$

$$S_g = \frac{F_O}{3(F_{CO} + F_{CH_4})} \quad (3)$$

where

S_{H_2} = Selectivity of H₂

S_g = Selectivity of CO and CH₄ Product Yield

$$Y_g(\%) = \frac{F_g}{3(F_{C_3H_8O_3, in})} \times 100\% \quad (4)$$

$$Y_{H_2}(\%) = \frac{2F_{H_2}}{8(F_{C_3H_8O_3, in})} \times 100\% \quad (5)$$

where

$$Y_{H_2} = \text{Yield of } H_2$$

$$Y_g = \text{Yield of CO or } CH_4$$

as well as the glycerol conversion to gaseous products based on the atom-H balance

$$X_{gly}(\%) = \frac{2 \times F_{H_2} + 4 \times F_{CH_4}}{8(F_{C_3H_8O_3,in})} \times 100\% \quad (6)$$

and
the reaction rate which was obtained by:

$$r_i \left(\text{mol g}^{-1} \text{s}^{-1} \right) = \frac{y_i \times F_{exit}}{W} \quad (7)$$

where

$$y_i = \text{dry basis composition of product } i$$

$$F_{exit} = \text{molar flow rate of gaseous products (mol s}^{-1}\text{)}$$

$$W = \text{weight of catalysts (g)}$$

3. Results and discussion

3.1. Catalyst characterization

Non-isothermal temperature-programmed calcination studies were carried out to obtain the air-solid sample interaction profile and the appropriate calcination temperature for the dried catalysts. Figs. 2 and 3 illustrate the weight loss and derivative weight profile of the 3 wt% La-promoted catalyst respectively. It can be observed that when the solid samples were heated, weight reductions were recorded symptomatic of the gas–solid interaction within a certain temperature region. Moreover, in the temperature region of 298–410 K, an average percentage weight loss of 13.0 wt % was recorded. This weight loss was most likely due to the removal of the physisorbed water and bulk water that were initially present in the sample. The second weight loss occurred within the temperature range of 430 to about 580 K (15.0 wt% loss). According to Estellé et al. [19], this weight loss can be attributed to the elimination of chemically bound water from nickel nitrate hexahydrate ($Ni(NO_3)_2 \cdot 6H_2O$) as in Eq. (8) as well as lanthanum nitrate hexahydrate ($La(NO_3)_3 \cdot 6H_2O$) as shown in Eq.

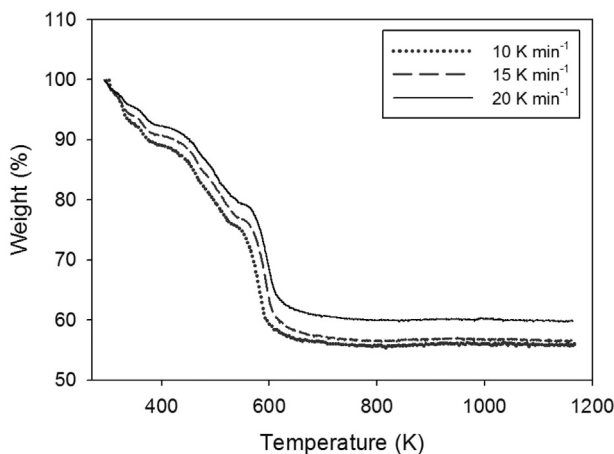


Fig. 2. Temperature-programmed calcination weight loss profile of the 3 wt% La-Ni/ Al_2O_3 catalyst.

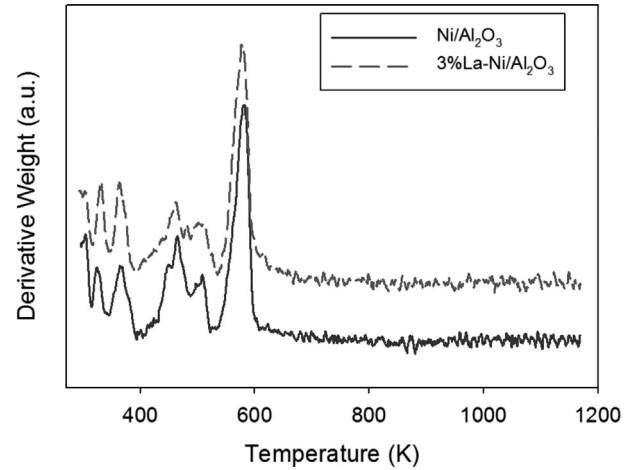
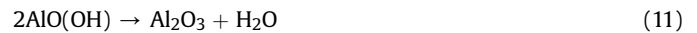
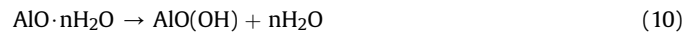
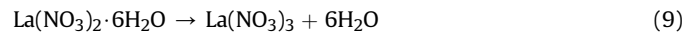
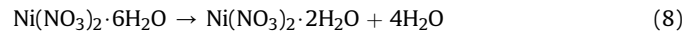


Fig. 3. Temperature-programmed calcination derivative weight profile.

(9). In addition, the Eqs. (10) and (11) may occur to release the water.



Finally, for the third temperature region (580–620 K), the weight loss of the sample was 16.0 wt% with a distinct derivative profile peak. The weight loss in this temperature region can be ascribed to the decomposition of nickel nitrate ($Ni(NO_3)_2 \cdot (OH)_2$) and lanthanum nitrate ($La(NO_3)_3$) to form La_2O_3 and NiO species respectively [20,21]. A further increase to the temperature has yielded flat profiles. This has indicated that a minimum temperature of 620 K was adequate for the calcination of catalysts for the actual reaction studies. Therefore, the calcination temperature employed in our current work, 1073 K as aforementioned, was sufficient to eradicate the nitrates for the creation of oxide-metals.

The modelling of non-isothermal calcination kinetics was further carried out via the model-free iso-conversion equations, viz. the Kissinger-Akahira-Sunose (KAS) (cf. Eq. (12)) and Flynn-Wall-Ozawa (FWO) models (cf. Eq. (13)) Eq. (13). It has been reported in the previous work [22] that both the aforementioned models can give reliable activation energy (E_a) estimations.

$$\ln \left(\frac{\beta}{T_a^2} \right) = \ln \frac{A_a R}{E_a g(\alpha)} - \frac{E_a}{RT_a} \quad (12)$$

$$\ln(\beta) = \ln \frac{A_a E_a}{R g(\alpha)} - 5.331 - 1.052 \frac{E_a}{RT_a} \quad (13)$$

where,

$$\beta = \text{apparent heating rate (K min}^{-1}\text{)},$$

$$A_a = \text{apparent pre-exponential factor (s}^{-1}\text{)},$$

$$E_a = \text{apparent activation energy (kJ mol}^{-1}\text{)},$$

$$T_a = \text{apparent temperature (K)},$$

$$R = \text{gas constant (J mol}^{-1} \text{K}^{-1}\text{)},$$

$$\alpha = \text{solid state conversion that can be estimated from } \alpha = \frac{W_i - W}{W_i - W_f}$$

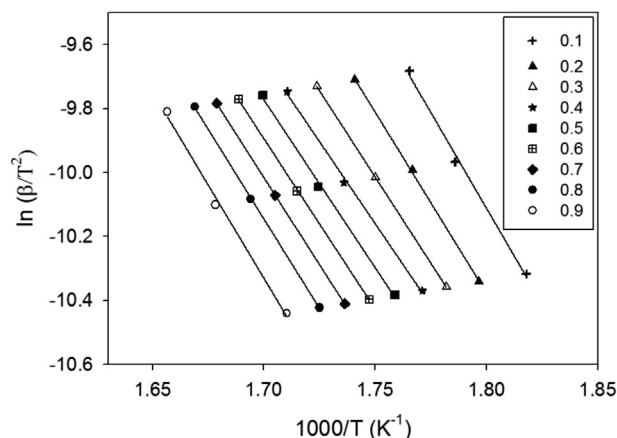


Fig. 4. Kissinger–Akahira–Sunose (KAS) profile for temperature-programmed calcination of the 3 wt% La–Ni/Al₂O₃ catalyst.

where

W = weight at instantaneous time (mg),

W_i = initial weight (mg),

W_f = final weight (mg).

Based on Figs. 4 and 5 (as representative), the KAS and FWO models were plotted against the α from 0.1 to 0.9. The same procedures were repeated for the different ramping rates (10, 15 and 20 K min^{−1}) to determine the E_a magnitude. Tables 1 and 2 summarize the results. The computed R^2 values have attained 0.99 indicative of a near-perfect fit. The obtained E_a values from the KAS and FWO models were within the range of 94.0–174.0 kJ mol^{−1} and 90.0–143.0 kJ mol^{−1} respectively. The results indicated that the activation energy was a function of α and each iso-conversion may represent a certain dominating mechanism step. Furthermore, it can also be observed from both Tables 1 and 2 that the 3.0 wt% La–Ni/Al₂O₃ catalyst consistently exhibited smaller E_a compared to the unpromoted Ni/Al₂O₃ catalyst indicating that the La-metal can actually promote the calcination process.

As shown in Table 3, the BET specific surface area of calcined alumina was 137.0 m² g^{−1}. Upon impregnation with Ni metal, the BET specific surface area was reduced to 85.0 m² g^{−1}. This may be due to the pore blockage by the metal addition. However, La doping

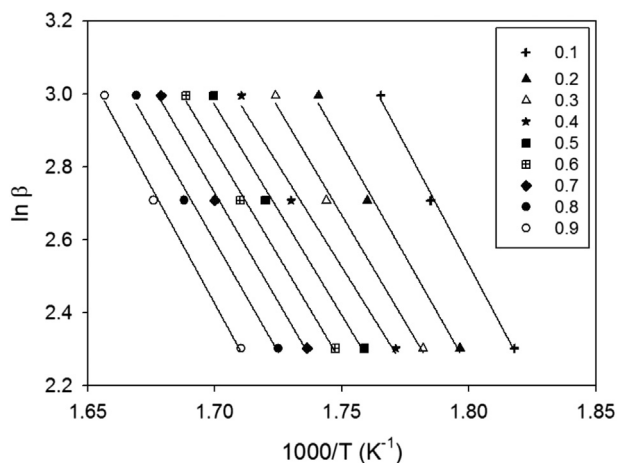


Fig. 5. Flynn–Wall–Ozawa (FWO) profile for temperature-programmed calcination of the 3 wt% La–Ni/Al₂O₃ catalyst.

Table 1

KAS modelling of the temperature-programmed calcination.

α	Ni/Al ₂ O ₃		3 wt% La–Ni/Al ₂ O ₃	
	E_a (kJ mol ^{−1})	R^2	E_a (kJ mol ^{−1})	R^2
0.1	126.44	0.99	115.39	0.98
0.2	137.19	0.99	111.26	0.99
0.3	142.04	0.99	104.40	0.99
0.4	130.78	0.99	104.57	0.99
0.5	126.72	0.99	103.22	0.99
0.6	120.16	0.99	104.50	0.99
0.7	119.84	0.98	105.26	0.99
0.8	114.47	0.99	104.81	0.99
0.9	110.12	0.99	114.49	0.99

Table 2

FWO modelling of the temperature-programmed calcination.

α	Ni/Al ₂ O ₃		3%La–Ni/Al ₂ O ₃	
	E_a (kJ mol ^{−1})	R^2	E_a (kJ mol ^{−1})	R^2
0.1	173.17	0.99	96.67	0.99
0.2	146.33	0.99	103.93	0.99
0.3	151.14	0.99	108.70	0.99
0.4	140.06	0.99	112.34	0.99
0.5	136.26	0.99	115.63	0.99
0.6	129.45	0.99	117.2	0.99
0.7	129.80	0.99	116.34	0.99
0.8	125.06	0.99	114.1	0.99
0.9	120.78	0.99	113.48	0.99

Table 3

The BET specific surface area of fresh catalysts.

Sample	BET specific surface area (m ² g ^{−1})
Alumina	136.9
Ni/Al ₂ O ₃	85.2
3wt% La–Ni/Al ₂ O ₃	96.0

at 3 wt% was able to increase the BET specific surface area, attaining a value of 96.0 m² g^{−1}. This may be due to the well-dispersed NiO species (confirmed by the subsequent XRD results) which has led to a smaller crystallite size by La dopant that has acted as a structural promoter.

The presence of NiO compound and its crystallite size of Ni/Al₂O₃ and La–Ni/Al₂O₃ catalyst have been determined via the XRD diffractogram analysis (cf. Fig. 6). The peak at 2θ of 43° can be assigned to the NiO species whilst the peaks recorded at 2θ of 37.0°,

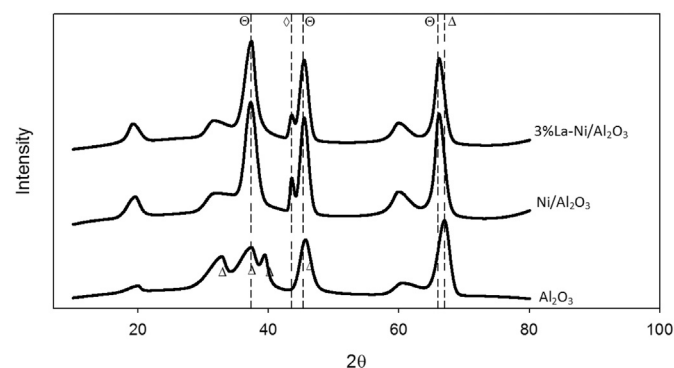


Fig. 6. XRD pattern of the prepared catalysts: (Δ) Al₂O₃, (◇) NiO and (Θ) NiAl₂O₄.

44.9° and 65.5° respectively can be attributed to the Ni/Al₂O₃ species. In addition, the particle size was estimated using Scherrer equation as in Eq. (14):

$$d = \frac{0.90\lambda}{\beta \cos \theta} \quad (14)$$

where d is the mean size (crystalline), λ is the x-ray wavelength, β represents the line broadening at half the maximum intensity in radian (FWHM) and θ is the Bragg angle. Based on the NiO diffracted peak, Table 4 shows that the La-promoted catalyst has a smaller crystallite size at 9.1 nm in comparison to the unpromoted Ni/Al₂O₃ catalyst (12.8 nm). Therefore, this has supported the earlier proposition of better metal particle dispersion and catalyst surface area increment with the incorporation of La metal.

The temperature-programmed reduction (TPR) analysis was carried out to determine the catalyst reducibility. As can be observed from Fig. 7, the TPR profile of the virgin alumina support is flat indicative of its inertness towards the H₂-reduction. In contrast, for both the Ni/Al₂O₃ and 3.0 wt% La–Ni/Al₂O₃ catalysts, two reduction peaks were observed viz. 700–800 K region and 800–850 K symptomatic of NiO reduction. Moreover, another peak was visible in the region of 850–1200 K that can be assigned to the NiAl₂O₄ spinel reduction. A previous study by Dieuzeide et al. [23] has also reported peaks in a similar temperature range for NiO (600–723 K and 773–1023 K regions) and NiAl₂O₄ (950–1123 K) reduction. Significantly, a slight shift of La-promoted Ni/Al₂O₃ catalyst to the lower temperature region in contrast to the unpromoted Ni/Al₂O₃ showed that La has enhanced the catalyst's reducibility.

3.2. Reaction studies

In the blank run studies (without the presence of the catalyst), insignificant amounts of products were formed indicative of a negligible gas-phase reforming reaction. Subsequently, in all the catalytic experiments, it was found that the H₂ and CO species constituted the primary products (syngas) of gaseous phase whilst some CH₄ was also co-produced over the 3wt% La–Ni/Al₂O₃ catalyst. Fig. 8(a) and (b) show the glycerol conversion (X_g), C₃H₈O₃ consumption rate, H₂ and CO formation rates as well as CH₄ formation rate as a function of CO₂-to-C₃H₈O₃ (CGR) ratio at 1023 K. At CGR of zero (pure glycerol), significant H₂ and CO formation rates were obtained (1.9×10^{-4} and 9.0×10^{-5} mol g⁻¹ s⁻¹ respectively) confirming that the catalytic glycerol decomposition has indeed occurred. Although initially the addition of CO₂ seems to increase the production rate of syngas consistent with the reaction proposition in the Eq. (1), the reaction trend has yielded maximum peaks for glycerol conversion, X_g (96.6%) and H₂ formation rate (2.4×10^{-4} mol g⁻¹ s⁻¹) at CGR of 1.67. Thereafter both X_g and H₂ production rate dropped with CGR at the region above 1.67. In contrast, the CO formation rate has continued to increase albeit slower at CGR greater than 1.67. Significantly, this can be ascribed to the shift in reaction mechanisms. At higher CGR, the dominating reaction could be gasification of the deposited carbon ($\text{CO}_2 + \text{C} \leftrightarrow 2\text{CO}$) that has offset the dwindling influence of glycerol dry reforming. On the other hand, the CH₄ formation rate has been on the decline before plateauing at CGR beyond 1.67 indicating that

Table 4

Crystallite size of the Ni/Al₂O₃ and the 3 wt% La-promoted Ni/Al₂O₃ catalysts from NiO peak.

Catalyst	Ni/Al ₂ O ₃	3 wt% La–Ni/Al ₂ O ₃
Crystallite size (nm)	12.8	9.1

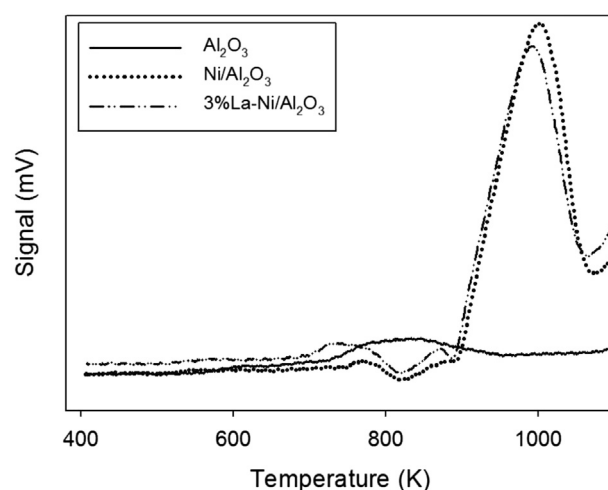


Fig. 7. TPR profiles of the fresh calcined catalysts.

the CH₄ could be originating directly from the glycerol decomposition and was consumed via the competing CH₄ dry reforming reaction ($\text{CH}_4 + \text{CO}_2 \leftrightarrow 2\text{H}_2 + 2\text{CO}$). In terms of product yield and selectivity, as can be seen in Table 5, the highest yield (%) of H₂ and

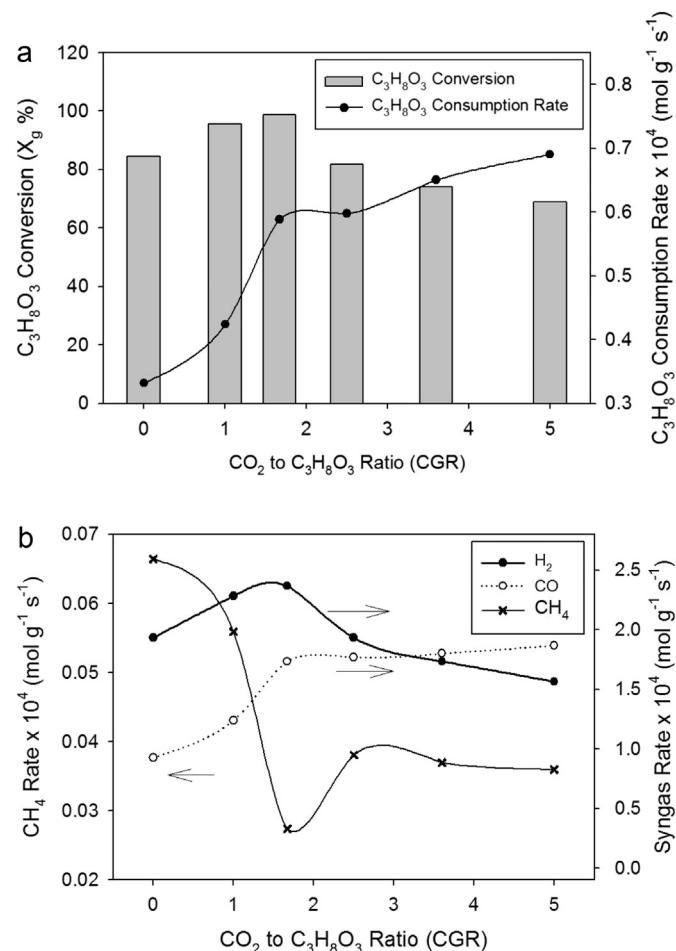


Fig. 8. a. Gaseous product formation rate over the 3wt% La–Ni/Al₂O₃ catalyst ($T = 1023$ K; $P = 1$ atm; $\text{GHSV} = 3.6 \times 10^{-4}$ ml g⁻¹ h⁻¹ STP). b. Glycerol conversion and glycerol consumption rate over the 3 wt% La–Ni/Al₂O₃ catalyst ($T = 1023$ K; $P = 1$ atm; $\text{WHSV} = 3.6 \times 10^{-4}$ ml g⁻¹ h⁻¹ STP).

Table 5
Yield and selectivity of products as a function of CGR at 1023 K.

CGR	Selectivity			Yield (%)		
	H ₂	CO	CH ₄	H ₂	CO	CH ₄
0	1.34	0.93	0.068	78.46	54.71	3.97
1	1.24	0.97	0.027	92.83	72.95	2.015
1.67	0.94	0.98	0.017	97.25	102.24	1.75
2.5	0.75	0.98	0.018	78.68	103.73	1.93
5	0.52	0.97	0.029	63.65	118.55	3.51

CO were 97% and 118% respectively whilst the H₂ and CO selectivity values were 0.93 and 0.98 respectively. In all cases, the selectivity and yield of CH₄ were always considerably lower than the rest. Significantly, as can be seen from Fig. 9, the obtained H₂:CO product ratios from the current work were always lower than 2.0, dropped from the 2.0 recorded at the CGR of zero to approximately 0.70 at the CGR of 5.0. In contrast, the syngas composition from the previous glycerol steam reforming works always yielded H₂:CO of more than 6.0 which rendered them unsuitable for Fischer-Tropsch synthesis [24,25].

The glycerol consumption rates were also obtained at 923 K and 1123 K in addition to the aforementioned 1023 K. The collected data sets were subsequently fitted with the power-law equation to obtain the kinetic parameters as shown in Eq. (15).

$$r_g = Ae^{\frac{-E_a}{RT}} (P_{C_3H_8O_3})^\gamma (P_{CO_2})^\phi \quad (15)$$

where

r_g = Glycerol consumption rate (mol g⁻¹ s⁻¹)

A = Exponential factor

E_a = Activation energy (kJ mol⁻¹)

R = Ideal gas constant

T = Temperature (K)

P_{CO_2} = CO₂ partial pressure (kPa)

$P_{C_3H_8O_3}$ = Glycerol partial pressure (kPa)

γ = Reaction order with respect to C₃H₈O₃

ϕ = Reaction order with respect to CO₂

For the modelling, the rate data associated with the pure glycerol decomposition was neglected during computation as the objective was to obtain global parameters that represent the dry

Table 6
Kinetic parameters of the glycerol consumption rate from the power law modelling.

Parameter	Value
A	2.6×10^{-4}
E_a (kJ mol ⁻¹)	34.9
γ	0.72
ϕ	0.14

reforming reaction. The resulting kinetics parameters from the fitting exercise are listed in Table 6. Significantly, the E_a over the 3wt%La–Ni/Al₂O₃ catalyst was 35.0 kJ mol⁻¹ whilst the γ was 0.72, an approximately five-folds larger than the ϕ (0.14). This showed that the P_{CO_2} offered lesser influence towards the overall glycerol consumption rate as compared to the $P_{C_3H_8O_3}$. Moreover, Fig. 10 shows the parity plot whereby the distribution of data was random. Therefore, the kinetics parameters obtained from the power law modelling were statistically adequate.

Significantly, a 72 h longevity study was carried out at 1023 K over the 3 wt% La catalyst and the trend is depicted in Fig. 11. The 3 wt% La catalyst has yielded stable performance with no apparent severe deactivation. The exit flow rate was averaging 190 ml min⁻¹. In addition, Fig. 12 reveals that the transient glycerol conversion, X_g (averaging 90.0%) as well as the product compositions for H₂ (30.0 mol%), CO (20.0 mol%) and CH₄ (1–2.0 mol%) were stable over the entire 72 h. Therefore, it can be concluded that the 3 wt% La–Ni/Al₂O₃ catalyst was able to catalyze glycerol dry reforming over an extended period of reaction without significant deactivation.

4. Conclusions

The results from glycerol dry reforming reaction over the 3 wt% La-promoted alumina supported Ni catalyst showed that copious amounts of H₂ and CO were produced with the attendant H₂:CO ratios which were always lower than 2.0. The syngas was primarily from glycerol decomposition pathway. At reaction temperature of 1023 K, H₂:CO ratios were in between 2.0 and 0.7 at CO₂-to-glycerol ratio of zero to five. The increasing CO formation rate with concomitant decrease in H₂ formation rate with CO₂-to-glycerol ratio seems to suggest that the CO₂ has also taken part in other reaction pathways, viz. the reverse-water-gas shift and carbon gasification. Significantly, the longevity study has revealed a stable

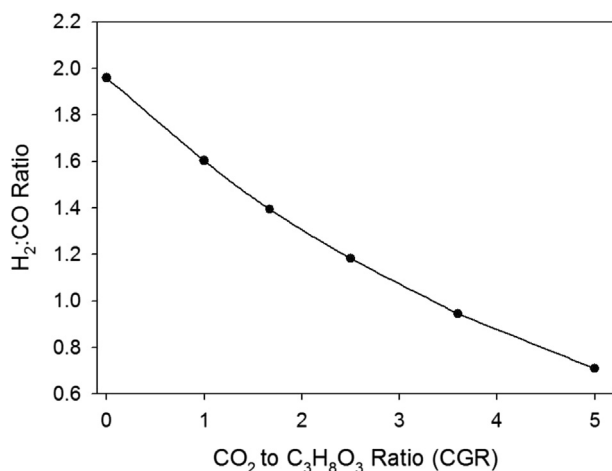


Fig. 9. H₂:CO ratio over 3wt% La–Ni/Al₂O₃ catalyst ($T = 1023$ K; $P = 1$ atm; WHSV = 3.6×10^{-4} ml g⁻¹ h⁻¹ STP).

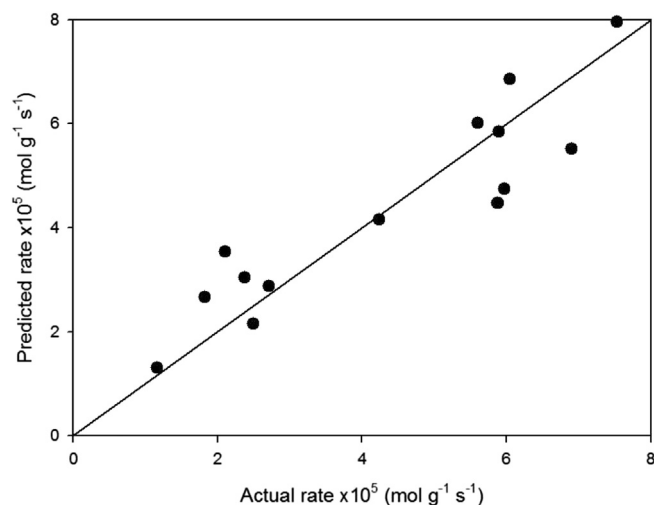


Fig. 10. Parity plot showing the predicted glycerol consumption rate versus the actual glycerol consumption rate.

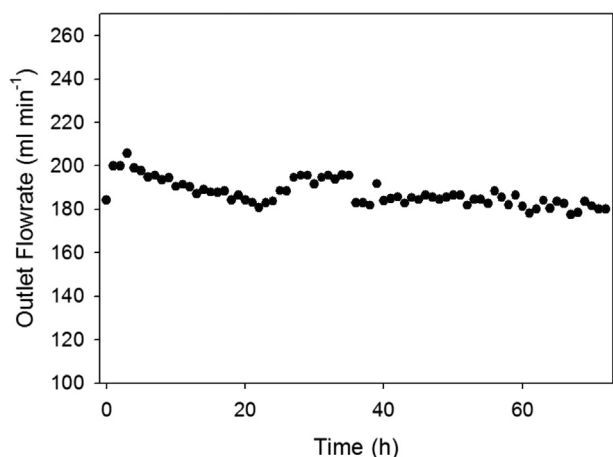


Fig. 11. Outlet flowrate during the 72 h longevity run over the 3wt% La–Ni/Al₂O₃ catalyst ($T = 1023$ K; $P = 1$ atm; WHSV = 3.6×10^{-4} ml g⁻¹ h⁻¹ STP).

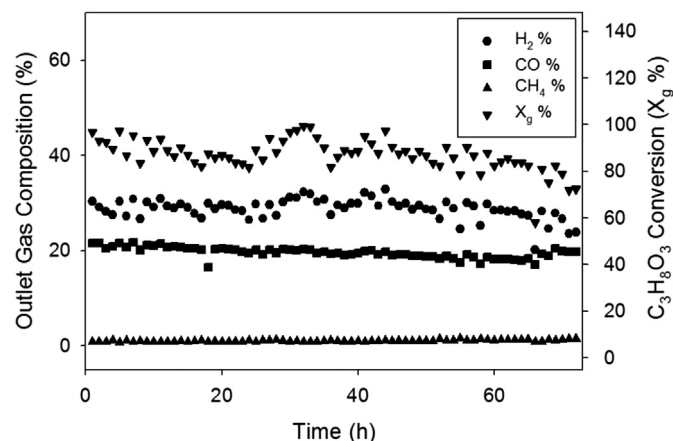


Fig. 12. Syngas (H₂ & CO), CH₄ composition and glycerol conversion during the 72 h longevity run over the 3wt% La–Ni/Al₂O₃ catalyst ($T = 1023$ K; $P = 1$ atm; WHSV = 3.6×10^{-4} ml g⁻¹ h⁻¹ STP).

reaction even after 72 h of continuous reaction at 1023 K. Moreover, the high glycerol conversions ($X_g = 90\%$) and a stable H₂:CO (1.2–1.7) product ratio over the extended reaction duration have supported the proposition that syngas product from the current work is more suitable for Fischer-Tropsch synthesis compared to the glycerol steam reforming pathway.

Acknowledgements

The authors would like to acknowledge financial support from the Ministry of Education, Malaysia through research grant RDU121216 (MTUN-CoE) and RDU140112 (FRGS). Kah Weng Siew is a grateful recipient of GRS120377 scholarship from the Universiti Malaysia Pahang.

References

- [1] Cheng CK, Foo SY, Adesina AA. Carbon deposition on bimetallic Co–Ni/Al₂O₃ catalyst during steam reforming of glycerol. *Catal Today* 2011;164:268–74.
- [2] Fernández Y, Menéndez JA. Influence of feed characteristics on the microwave-assisted pyrolysis used to produce syngas from biomass wastes. *J Anal Appl Pyrol* 2011;91:316–22.
- [3] Kale GR, Kulkarni BD. Thermodynamic analysis of dry autothermal reforming of glycerol. *Fuel Process Technol* 2010;91:520–30.
- [4] Mikhailov YM, Kustov LM, Aleshin VV, Tarasov AL, Leonova VN. Steam reforming of glycerol over composites containing nickel nanoparticles. *Catal Ind* 2011;3(2):189–91.
- [5] Foo SY, Cheng CK, Nguyen TH, Kennedy EM, Dlugogorski BZ, Adesina AA. Carbon deposition and gasification kinetics of used lanthanide-promoted Co–Ni/Al₂O₃ catalysts from CH₄ dry reforming. *Catal Commun* 2012;26:183–8.
- [6] Pant KK, Jain R, Jain S. Renewable hydrogen production by steam reforming of glycerol over Ni/CeO₂ catalyst prepared by precipitation deposition method. *Korean J Chem Eng* 2011;28(9):1859–66.
- [7] Hasin P, Koonsaeng N, Laobuthee A. Nickel–aluminium complex: a simple and effective precursor for nickel aluminate (NiAl₂O₄) spinel. *Maejo Int J Sci Tech* 2008;2(1):140–9.
- [8] Cheng CK, Foo SY, Adesina AA. H₂-rich synthesis gas production over Co/Al₂O₃ catalyst via glycerol steam reforming. *Catal Commun* 2010;12:292–8.
- [9] Sechested J, Gelten JAP, Remedakis IN, Bengaard H, Nørskov JK. Sintering of nickel steam-reforming catalysts: effects of temperature and steam and hydrogen pressures. *J Catal* 2004;223:432–43.
- [10] Choi JS, Moon KI, Kim YG, Lee JS, Kim CH, Trimm DL. Stable carbon-dioxide reforming of methane over modified Ni/Al₂O₃ catalysts. *Catal Lett* 1998;52:43–7.
- [11] Jiang PB, Shang YC, Cheng TX, Bi YL, Shi KY, Wei SQ, et al. Methane decomposition over Ni/α-Al₂O₃ promoted by La₂O₃ and CeO₂. *J Nat Gas Chem* 2003;12:183–8.
- [12] Natesakhawat S, Watson RB, Wang XQ, Ozkan US. Deactivation characteristics of lanthanide-promoted sol-gel Ni/Al₂O₃ in propane steam reforming. *J Catal* 2005;234:496–508.
- [13] Seo JG, Youn MH, Jung JC, Song IK. Effect of preparation method of mesoporous Ni–Al₂O₃ catalysts on their catalytic activity for hydrogen production by steam reforming of liquefied natural gas (LNG). *Int J Hydrog Energy* 2009;34(9):5409–16.
- [14] Sutthiumporn K, Kawi S. Promotional effect of alkaline earth over Ni–La₂O₃ catalyst for CO₂ reforming of CH₄: role of surface oxygen species on H₂ production and carbon suppression. *Int J Hydrog Energy* 2011;36:14435–46.
- [15] Lucrécio AF, Jerkiewicz G, Assaf EM. Nickel catalysts promoted with cerium and lanthanum to reduce carbon formation in partial oxidation of methane reactions. *Appl Catal A Gen* 2007;333(1):90–5.
- [16] Dan M, Lazar MD, Rednic V, Almasan V. Methane steam reforming over Ni/Al₂O₃ promoted by CeO₂ and La₂O₃. *Rev Roum Chim* 2011;56(6):643–9.
- [17] Bang YJ, Seo JG, Song IK. Hydrogen production by steam reforming of liquefied natural gas (LNG) over mesoporous Ni–La–Al₂O₃ aerogel catalysts: effect of La content. *Int J Hydrog Energy* 2011;36(14):8307–15.
- [18] Gao J, Hou ZY, Lou H, Zheng XM. Dry (CO₂) reforming. In: Shekhwat D, Spivey JJ, Berry DA, editors. *Fuel cells*. Amsterdam: Elsevier; 2011. p. 191–221.
- [19] Estellé J, Salagre P, Cesteros Y, Serra M, Medina F, Sueiras JE. Comparative study of the morphology and surface properties of nickel oxide prepared from different precursors. *Solid State Ionics* 2003;156:233–43.
- [20] Abayomi JA, Raphael OI, Ajay KD. Synthesis, characterization and performance evaluation of Ni/Al₂O₃ catalysts for reforming of crude ethanol for hydrogen production. *Appl Catal A Gen* 2005;287:159–75.
- [21] Behera SK, Sahu PK, Pratihari SK, Bhattacharyya S. Low temperature synthesis of spherical lanthanum aluminate nanoparticles. *Mat Lett* 2004;58:3710–5.
- [22] Słopiecka K, Bartocci P, Fantozzi F. Thermogravimetric analysis and kinetic study of poplar wood pyrolysis. *Appl Energy* 2012;97:491–7.
- [23] Dieuzeide ML, Iannibelli V, Jobbagy M, Amadeo N. Steam reforming of glycerol over Ni/Mg/γ-Al₂O₃ catalysts. Effect of calcination temperatures. *Int J Hydrog Energy* 2012;37:14926–30.
- [24] Mastalir A, Frank B, Szizybalski A, Soerijanto H, Deshpande A, Niederberger M, et al. Steam reforming of methanol over Cu/ZrO₂/CeO₂ catalysts: a kinetic study. *J Catal* 2005;230(2):464–75.
- [25] Pompeo F, Santoro G, Nichio NN. Hydrogen and/or syngas from steam reforming of glycerol. Study of platinum catalysts. *Int J Hydrog Energy* 2010;35:8912–20.